Local resonator with high-static-low-dynamic stiffness for lowering band gaps of flexural wave in beams

Jiaxi Zhou,[1,a)] Kai Wang,[1] Daolin Xu,[1,2] and Huajiang Ouyang[3]

[1] *College of Mechanical and Vehicle Engineering, Hunan University, Changsha 410082, PR China*

[2] *State Key Laboratory of Advanced Design and Manufacturing for Vehicle Body Changsha 410082, PR China*

[3] *School of Engineering, University of Liverpool, Liverpool L69 3GH, UK*

Periodic structures are effective in attenuating wave in low frequency range at local resonance (LR) conditions, but it is still a challenge to achieve this in very low frequency range. The main original contribution of this paper is to further lower the band gaps of flexural wave propagation in LR beams by developing a new resonator with high-static-low-dynamic stiffness (HSLDS). The proposed resonator is designed by combining a vertical spring with two oblique springs that provide negative stiffness in the vertical direction, and thus the stiffness of the vertical spring can be counteracted effectively by the negative-stiffness (NS) mechanisms. The band structures of HSLDS-LR beams, obtained by the transfer matrix method and verified by numerical simulations, demonstrate that band gaps can be shifted to much lower frequency than that of conventional LR beams. Most importantly, the band gaps can be assigned to desired locations by adjusting only the stiffness of the oblique springs. For wave attenuation in HSLDS-LR beams with finite length, a sufficient number of unit cells are required to achieve a good performance of attenuation.

I. INTRODUCTION

Phononic crystals comprised of periodic materials or structures have drawn extensive attention from researchers, due to their fascinating features, including the capability of attenuating waves in a certain frequency range, called a stop band or a band gap, by tailoring the size or structure of the unit cell[1-8]. Generally, there are two mechanisms to create a band gap, either Bragg scattering (BS)[1] or local resonance (LR)[5]. The band gap of Bragg-type phononic crystals normally appear at a frequency with the same order of magnitude as the ratio of the wave velocity to the lattice constant[1], and thus ultra-large lattice constants are needed to control vibration wave propagation in machines and structures[5, 9], which are often unrealizable. Fortunately, the local resonance mechanism breaks through the dependence on wavelengths of the BS mechanism, and the band gap of such a mechanism merely depends on the resonant frequency of the local resonator[5, 7], which successfully shifts the band gap into low-frequency range. Since the design concept of local resonance was proposed, a large amount of work in this filed has been carried out, as well documented in the comprehensive review article by Hussein et al.[7] and the monograph

a) Author to whom correspondence should be addressed. Electronic mail: jxizhou@hnu.edu.cn.

edited by Deymier[8]. In this paper, we mainly focus on the attenuation of flexural waves in LR beams, and thus a brief literature review related to this topic is given as follows.

Yu et al.[9, 10] studied band gaps of flexural waves in LR beams by using transfer matrix theory and experimental tests, where the local resonator was realized by composing a soft rubber ring and a copper ring. For such LR beams, Liu et al.[11] discussed parametric factors that affect the attenuation property, and Xiao et al.[12] analytically studied the formation mechanism of band structures. Chen et al.[13] embedded local resonators into sandwich beams to attenuate flexural wave propagation in them. In order to broaden the width of the band gap, Xiao et al.[14] proposed multiple periodic arrays of local resonators with mismatching resonant frequencies, and Zhu et al.[15] used this design concept to construct a chiral metamaterial beam for vibration suppression. Badreddine Assouar and Oudich[16] extended stub-type resonators attached onto host plates from one side to double sides to achieve broader band gaps. An alternative way to achieve wide band gaps might be constructing a resonator with multiple degrees of freedom (DOF). Xiao et al.[17] investigated band structures of flexural wave in beams with beam-like resonators, which revealed some new features of band gaps, e.g. transition and near-coupling effects between BS band gaps and LR ones. Wang et al. proposed a two-DOF resonator[18] and a continuum-beam resonator[19] for attenuating flexural wave in LR beams, and both investigations indicated wide band gaps. Pai et al.[20] proposed a two-stage resonator with different stiffness and mass in each layer to achieve two band gaps. Wang et al.[21] obtained multiple band gaps of flexural waves in LR beams by using resonators attached with lateral oscillators. On the other hand, piezoelectric shunts were periodically installed onto host structures as tunable resonators for broadband vibration and wave propagation control of flexible plates[22, 23].

Compared with broadening band gaps, lowering band gaps to handle the tough issue of controlling very low frequency wave propagation in structures is probably a more attractive topic. The frequency range of the band gap of an LR beam is determined by the resonant frequency of the resonator, and thus a direct route of lowering band gaps might be reducing the resonant frequency, which was generally realized, for example, by using a heavy core coated with soft materials [5], or a metal solid cylinder suspended by a soft cylinder (stub)[24, 25]. Nouh et al.[26] studied flexural wave propagation in a slender beam with periodic holes that are filled with membranes attached with small lumped masses, which showed low-frequency band gaps. Some researchers resorted to weakening host structures of phononic crystals, e.g. Bilal and Hussein[27] and Badreddine Assouar et al.[28] punched holes periodically on a host plate, which made solid regions act as springboards of a resonator (pillars act as heavy masses), leading to lower and broader band gaps. However, the above methods might be unworkable when one faces the issue of wave attenuation at very low frequency in host structures that cannot or are not

allowed to be weakened, due to a fact that it is unrealizable to make the stiffness of a resonator ultra-low, or the mass ultra-large. Therefore, it is still a challenge to realize wave attenuation by LR phononic crystals in very low frequency range[7].

The motivation of this paper is to substantially lower band gaps of flexural wave in LR beams by developing a new resonator with high-static-low-dynamic stiffness (HSLDS), called HSLDS resonator for brevity. The elastic element of the resonator is constructed by combining a vertical spring with two oblique springs, which act as a mechanism to provide negative stiffness in the vertical direction[29, 30], and thus the stiffness of the vertical spring can be effectively counteracted by the negative-stiffness (NS) mechanism. It should be noted that the additional NS mechanism cannot degrade the capability of suspending a heavy mass, because oblique springs are horizontal and thus perpendicular to the vertical spring at the static equilibrium, and thus the mass is completely suspended by the vertical spring. Therefore, this type of resonator possesses the excellent property of high static but low dynamic stiffness. More importantly, the stiffness of the resonator (i.e., the residual stiffness after counteraction by the NS mechanisms) can be tuned to desired values by just adjusting the stiffness of oblique springs. Consequently, the band gaps of flexural waves in LR beams can be shifted towards a very low frequency. It is worth noting that the stiffness is nonlinear; however, design optimization is carried out to reduce the degree of nonlinearity as far as possible, and thus keep a mainly linear property of the stiffness when the structures do not undergo large displacements. In such case, the linearized stiffness is adopted in the theoretical analysis by using the transfer matrix method, but the nonlinear stiffness in numerical simulations in all cases. Additionally, effects of excitation amplitudes on the band structure and influences of the number of unit cells on attenuation are analyzed.

This paper is organized as follows. The propagation of flexural wave in beams with HSLDS resonators is analyzed in Section II, including design of a HSLDS resonator, demonstrations of band gaps obtained based on Floquet-Bloch theorem, and verifications of band gaps in terms of frequency response function (FRF) calculated by using the Galerkin method. And then the corresponding numerical experiments are given in Section III. Section IV presents the effects of the number of unit cells on wave attenuation in the band gap, and the impacts of degrees of nonlinearity on band structures. Finally, several conclusions are drawn in Section V.

II. Model and method of calculation

The physical model of an Euler-Bernoulli beam coupled with HSLDS resonators is shown in Fig. 1a, which is called HSLDS-LR beam for brevity in this paper. Each resonator is fixed onto the beam using a bolted joint and is constructed by combining a vertical spring with two oblique spring that provide negative stiffness in the vertical direction, as shown in Fig. 1b. It should be noted that the oblique springs are initially horizontal when the mass is fully supported by the vertical spring. One end of the vertical spring is screwed into a connector fixed on a rigid frame, while the other end is screwed into a

connector fixed on the mass. A linear bearing is embedded into the mass, which allows the mass to slide freely on the guide rod, to guarantee that the mass only oscillates along the vertical direction. Two ends of the oblique spring are hinged on the mass and the rigid frame, respectively. Inside each oblique spring, there is a guide rod sliding on a linear bearing to prevent it from possible bending and buckling. In order to maintain enough rigidity of the frame, there are triangle-shaped ribs reinforcing at two corners of the frame. Fig. 1c shows the computational model of the HSLDS-LR beam with infinite length, which is used to analyze the propagation of flexural waves in the HSLDS-LR beam by using the transfer matrix method based on Floquet-Bloch theorem. Finally, the dynamic equations of the HSLDS-LR beam with finite length are established, and the frequency response functions (FRFs) under free-free boundary condition are obtained to verify the band structures.

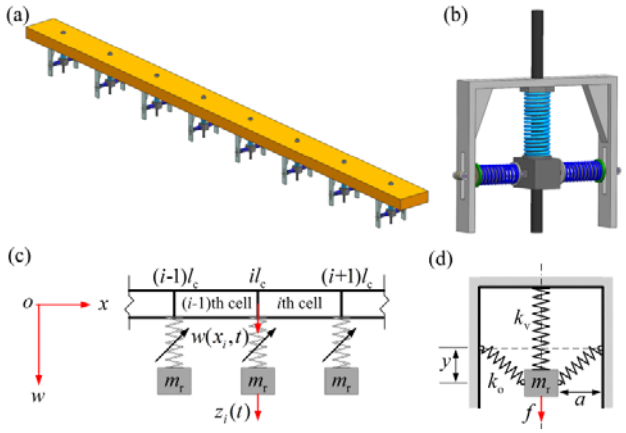

FIG. 1. (a) Physical model of the HSLDS-LR beam, (b) physical model of the HSLDS resonator, (c) computational model of the HSLDS-LR beam with infinite length, and (d) schematic diagram of static analysis of the HSLDS resonator.

A. Design of a HSLDS resonator

The HSLDS resonator is shown in Fig. 1b. Two oblique springs provide negative stiffness in the vertical direction when the mass oscillates around the equilibrium position, which is utilized to counteract the positive stiffness of the vertical spring. The mass can only oscillates along the vertical direction, and the oblique springs deform symmetrically with respect to the vertical spring. The restoring force of the HSLDS resonator can be obtained by static analysis, as shown in Fig. 1d,

$$f = k_v y - 2k_o y\left(\frac{l}{\sqrt{a^2 + y^2}} - 1\right) \tag{1}$$

where f is the restoring force; y is the displacement of the mass deviating from the static equilibrium position, as represented by the dashed horizontal line in Fig. 1d; k_v and k_o are the stiffness of vertical and oblique springs, respectively; l is the original length of oblique spring; a is the deformed length of oblique spring at the static equilibrium position, and $a < l$. Using $\bar{f} = f/k_v l$, $\bar{y} = y/l$, the non-dimensional restoring force can be written as

$$\bar{f} = \bar{y} - 2\alpha\bar{y}\left(\frac{1}{\sqrt{\bar{a}^2 + \bar{y}^2}} - 1\right) \tag{2}$$

where $\alpha = k_o / k_v$. As mentioned previously, the stiffness of the vertical spring can be partly or totally counteracted by the NS mechanisms. Let η ($0 \le \eta \le 1$) denotes the proportion of the residual stiffness of the resonator at its static equilibrium position in the vertical direction, after counteraction by the NS mechanisms, and then the restoring force can be rewritten as

$$\bar{f} = \eta\bar{y} + (1-\eta)\bar{y} - 2\alpha\bar{y}\left(\frac{1}{\sqrt{\bar{a}^2 + \bar{y}^2}} - 1\right) \tag{3}$$

The non-dimensional stiffness of the HSLDS resonator is derived by differentiating the above expression with respect to $\bar{y}$,

$$\bar{k} = \eta + (1-\eta) - 2\alpha\left[\frac{\bar{a}^2}{\left(\bar{a}^2 + \bar{y}^2\right)^{\frac{3}{2}}} - 1\right] \tag{4}$$

where $\bar{k} = k / k_v$, and k is the dimensional stiffness of the resonator. In order to reduce the stiffness of the resonator, and thus lower the band gap, one can counteract the stiffness by a ratio of $1-\eta$ by letting

$$(1-\eta) - 2\alpha\left[\frac{\bar{a}^2}{\left(\bar{a}^2 + \bar{y}^2\right)^{\frac{3}{2}}} - 1\right] = 0 \tag{5}$$

By doing this, at the static equilibrium $\bar{y}=0$, the non-dimensional stiffness of the resonator is successfully reduced from 1 to η , and the dimensional one from k_v to ηk_v . At $\bar{y}=0$, there is a unique relation between parameters η , α , and $\bar{a}$

$$\alpha = \frac{(1-\eta)\bar{a}}{2(1-\bar{a})} \tag{6}$$

which provides a physical expression of η related to parameters k_v , k_o , a and l . Substituting Eq. (6) into Eq. (3) and Eq. (4), one can obtain the restoring force and stiffness of the HSLDS resonator after a part of stiffness is counteracted by the ratio of $1-\eta$, as given below

$$\bar{f} = \left\{1 - (1-\eta)\frac{\bar{a}}{1-\bar{a}}\left(\frac{1}{\sqrt{\bar{a}^2 + \bar{y}^2}} - 1\right)\right\}\bar{y} \tag{7}$$

$$\bar{k} = 1 - (1-\eta)\frac{\bar{a}}{1-\bar{a}}\left(\frac{\bar{a}^2}{\left(\bar{a}^2 + \bar{y}^2\right)^{\frac{3}{2}}} - 1\right) \tag{8}$$

Note that, only at the static equilibrium $\bar{y}=0$, the stiffness is $\bar{k} = \eta$, and it increases as the displacement $\bar{y}$ increases. In order to lower the stiffness and reduce the degree of nonlinearity in the neighborhood of the equilibrium point as far as possible, the displacement range corresponding to the non-dimensional stiffness smaller than 1 should be maximized [30], i.e.

$$\text{Max.} \quad \bar{y}_d = \sqrt{\bar{a}^{\frac{4}{3}} - \bar{a}^2} \tag{9}$$

One can easily obtain its solution as $\bar{a}_{\text{opt}}=(2/3)^{3/2}$, leading to $\bar{y}_{\text{d max}}=2\sqrt{3}/9$, which means that the stiffness of HSLDS resonator is lower than that of its counterpart without the NS mechanisms in the displacement range of $-2\sqrt{3}/9l<y<2\sqrt{3}/9l$.

The stiffness of the HSLDS resonator with different proportions of residual stiffness is depicted in Fig.2, when $\bar{a}=(2/3)^{3/2}$. Obviously, the stiffness can be effectively designed to a desired value by adding the NS mechanisms. All the stiffness curves pass through two points $(\pm\bar{y}_{\text{d max}},1)$, which implies that the optimal $\bar{a}$ is independent of η. Additionally, when η is selected to be 1, the HSLDS resonator degrades to a linear one. Therefore, the proposed HSLDS resonator has a tunable feature of controlling the resonant frequency by changing its stiffness, which is desirable for phononic structures[7]. Also shown is that the stiffness of the NS resonator is close to η in the displacement range around the equilibrium point $\bar{y}$=0. Consequently, under circumstances of weak oscillations, the linearized stiffness can be used to analyze the propagation of flexural waves in HSLDS-LR beams using the transfer matrix method.

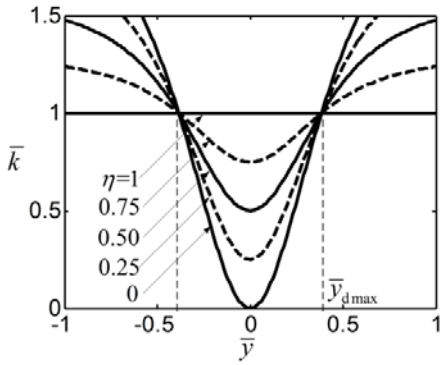

FIG. 2. Stiffness of the HSLDS-LR oscillator, when $\bar{a}=(2/3)^{3/2}$.

B. Propagation of flexural wave in HSLDS-LR beam with infinite length by transfer matrix method

The governing equation of motion of an Euler-Bernoulli beam can be given by

$$EI\frac{\partial^4 w}{\partial x^4}+\rho A\frac{\partial^2 w}{\partial t^2}=0 \tag{10}$$

where EI is the flexural rigidity, ρ the density, A area of cross section, and $w(x,t)$ is the dynamic transverse deflection at x. It is assumed that $w(x,t)=W(x)e^{\sqrt{-1}\omega t}$, where $W(x)$ is the mode shape function, which can be written as

$$W(x)=A\cos(\beta x)+B\sin(\beta x)+C\cosh(\beta x)+D\sinh(\beta x) \tag{11}$$

where A, B, C, and D are unknown coefficients, β is the flexural wavenumber and $\beta^4=\frac{\rho A}{EI}\omega^2$. For the ith unit cell, $W_i(x)$ can be written as

$$W_i(x')=A_i\cos(\beta x')+B_i\sin(\beta x')+C_i\cosh(\beta x')+D_i\sinh(\beta x') \tag{12}$$

where $x'=x-il_c$, $il_c \le x \le (i+1)l_c$, and l_c is the length of a unit cell, namely lattice constant.

Note that the situation of small-amplitude oscillations is considered here to study the wave propagation in this beam using the transfer matrix method, and thus the linearized stiffness at the static equilibrium ηk_v is adopted for the HSLDS resonator. The governing equation of the ith resonator can be given by

$$m_r\ddot{z}_i(t)+f(x_i,t)=0 \tag{13}$$

where $f(x_i,t)=-\eta k_v\left[w(x_i,t)-z_i(t)\right]$ is the internal force between the resonator and the beam at the connecting point. It can be assumed that $z_i(t)=Z_i e^{\sqrt{-1}\omega t}$, where Z_i is the displacement amplitude. Substituting this expression into Eq. (13), one can obtain

$$Z_i=\frac{\eta k_v W_i(0)}{\eta k_v-m_r\omega^2} \tag{14}$$

and thus $f(x_i,t)$ can be given by

$$f(x_i,t)=-\eta k_v\left[W_i(0)-Z_i\right]e^{\sqrt{-1}\omega t}=\frac{\eta k_v m_r\omega^2}{\eta k_v-m_r\omega^2}W_i(0)e^{\sqrt{-1}\omega t}=F_i e^{\sqrt{-1}\omega t} \tag{15}$$

where F_i is the amplitude of the internal force.

Considering the continuities of displacement, slope, bending moment and shear force at the connection point of the resonator, one can obtain

$$\begin{cases} W_{i-1}(l_c)=W_i(0) \\ W'_{i-1}(l_c)=W'_i(0) \\ EIW''_{i-1}(l_c)=EIW''_i(0) \\ EIW'''_{i-1}(l_c)+F_i=EIW'''_i(0) \end{cases} \tag{16}$$

Substituting Eq. (12) and Eq. (15) into Eq. (16) gives

$$\mathbf{H}\boldsymbol{\psi}_{i-1}=\mathbf{G}\boldsymbol{\psi}_i \tag{17}$$

where $\boldsymbol{\psi}_i=\{A_i, B_i, C_i, D_i\}^{\mathrm{T}}$ and

$$\mathbf{H}=\begin{bmatrix} \cos(\beta l_c) & \sin(\beta l_c) & \cosh(\beta l_c) & \sinh(\beta l_c) \\ -\beta\sin(\beta l_c) & \beta\cos(\beta l_c) & \beta\sinh(\beta l_c) & \beta\cosh(\beta l_c) \\ -\beta^2\cos(\beta l_c) & -\beta^2\sin(\beta l_c) & \beta^2\cosh(\beta l_c) & \beta^2\sinh(\beta l_c) \\ \beta^3\sin(\beta l_c) & -\beta^3\cos(\beta l_c) & \beta^3\sinh(\beta l_c) & \beta^3\cosh(\beta l_c) \end{bmatrix} \tag{18}$$

$$\mathbf{G}=\begin{bmatrix} 1 & 0 & 1 & 0 \\ 0 & \beta & 0 & \beta \\ -\beta^2 & 0 & \beta^2 & 0 \\ -F & -\beta^3 & -F & \beta^3 \end{bmatrix} \tag{19}$$

$$F=\frac{1}{EI}\frac{\eta k_v m_r\omega^2}{\eta k_v-m_r\omega^2} \tag{20}$$

According to the Floquet-Bloch theorem[1], for a one-dimensional periodic structure, one can obtain following relationship between $\boldsymbol{\psi}_{i\text{-}1}$ and $\boldsymbol{\psi}_i$

$$\boldsymbol{\psi}_i = e^{\sqrt{-1}ql_c}\boldsymbol{\psi}_{i\text{-}1} \tag{21}$$

where q is the wave vector, appearing as the form of scalar for one-dimension wave propagation. Substituting Eq. (21) into Eq. (17) gives

$$\left(\mathbf{G}^{-1}\mathbf{H} - e^{\sqrt{-1}ql_c}\mathbf{I}\right)\boldsymbol{\psi}_{i-1} = 0 \tag{22}$$

where $\mathbf{I}$ is the identity matrix. Then the dispersion relation of the NS-LR beam can be derived

$$\left|\mathbf{G}^{-1}\mathbf{H} - e^{\sqrt{-1}ql_c}\mathbf{I}\right| = 0 \tag{23}$$

For a given ω, one can obtain solutions of the wave vector q. The propagation of a flexural wave in the beam is dampened when the solution of q is imaginary, namely stop band or band gap. In contrast, the flexural wave propagates through the beam when the solution is real, namely pass band[9].

C. Dynamics of the HSLDS-LR beam with finite length

In order to analyze propagation characteristics of a beam with finite-length *L* and verify band structures obtained by the above elastodynamic analysis, the frequency response function (FRF) is adopted to determine the band gap. Generally, the FRF is defined as the spectrum of the output signal divided by that of the input signal. In the present paper, a vertical random (white noise) force with bandwidth from 1 to 800 Hz is applied at the left end of the beam. The displacement time histories at the left hand (*x*=0) are collected as the input signal, and those at the right hand (*x*=*L*) as the output signal. The dynamic responses are calculated by using the Galerkin method.

The governing equation of the HSLDS-LR beam can be given by

$$EI\frac{\partial^4 w}{\partial x^4} + \rho A\frac{\partial^2 w}{\partial t^2} = f_{\mathrm{R}}(t)\delta(x-0) + \sum_{i=1}^{n} f(x_i,t)\delta(x-x_i) \tag{24}$$

where $f_{\mathrm{R}}(t)$ is the random (white noise) force within a bandwidth form 1 to 800 Hz, and its expectation of amplitudes of frequency components is denoted by $\mathrm{Ex}(f_{\mathrm{R}})$, called amplitude expectation for brevity, and

$$f(x_i,t) = k_{\mathrm{v}}\left[z_i(t) - w(x_i,t)\right]\left\{1 - (1-\eta)\frac{\overline{a}}{1-\overline{a}}\left(\frac{1}{\sqrt{\overline{a}^2 + \left(\left[z_i(t) - w(x_i,t)\right]/l\right)^2}} - 1\right)\right\} \tag{25}$$

It is reminded that $w(x_i,t)$ is the transverse displacement of the beam at the connecting point of the *i*th resonator, and $z_i(t)$ is the vertical displacement of the *i*th resonator.

The Galerkin method is utilized to discretize the system, and thus $w(x,t)$ can be assumed to be

$$w(x,t)=\sum_{j=1}^{N}\phi_j(x)\,p_j(t) \tag{26}$$

where $\phi_j(x)$ are trail functions, and $p_j(t)$ are the generalized displacements. Substituting Eq. (26) into Eq. (24) gives

$$EI\sum_{j=1}^{N}\phi_j^{(4)}(x)\,p_j(t)+\rho A\sum_{j=1}^{N}\phi_j(x)\,\ddot{p}_j(t)=f_{\mathrm{R}}(t)\delta(x-0)+\sum_{i=1}^{n}f(x_i,t)\delta(x-x_i) \tag{27}$$

where

$$f(x_i,t)=k_{\mathrm{v}}\left[z_i(t)-\sum_{j=1}^{N}\phi_j(x_i)\,p_j(t)\right]\left\{1-(1-\eta)\frac{\bar{a}}{1-\bar{a}}\left(\frac{1}{\sqrt{\bar{a}^2+\left(\left[z_i(t)-\sum_{j=1}^{N}\phi_j(x_i)\,p_j(t)\right]\Big/l\right)^2}}-1\right)\right\} \tag{28}$$

Multiplying Eq. (27) by the weight functions $\varphi_j(x)$ and integrating it from 0 to L, one can obtain

$$\begin{aligned}&EI\sum_{j=1}^{N}\int_0^L\phi_j^{(4)}(x)\varphi_j(x)\mathrm{d}x\,p_j(t)+\rho A\sum_{j=1}^{N}\int_0^L\phi_j(x)\varphi_j(x)\mathrm{d}x\,\ddot{p}_j(t)\\&\quad=\int_0^L\varphi_j(x)\delta(x-0)\mathrm{d}x\,f_{\mathrm{R}}(t)+\sum_{i=1}^{n}\int_0^L\varphi_j(x)\delta(x-x_i)\mathrm{d}x\,f(x_i,t)\end{aligned} \tag{29}$$

In this paper, both the trail and weight functions are selected as the mode functions of the Euler-Bernoulli beam. The free-free end boundary condition is considered here, namely no limitations are applied on both ends, and thus the beam can vibrate freely. The mode functions of Euler-Bernoulli beam with free-free end can be found in Rao[31]

$$\phi_j(x)=\varphi_j(x)=\sin(\beta_j x)+\sinh(\beta_j x)+\frac{\sin(\beta_j L)-\sinh(\beta_j L)}{\cosh(\beta_j L)-\cos(\beta_j L)}\left[\cos(\beta_j x)+\cosh(\beta_j x)\right] \tag{30}$$

The wave number β defined below Eq. (11) can be determined from the following frequency equation

$$\cos(\beta_j L)\cosh(\beta_j L)=1 \tag{31}$$

Considering the orthogonality of mode functions, and taking into account modal damping and damping of resonators, Eq. (29) can be rewritten as

$$m_j\ddot{p}_j+c_j\dot{p}_j+k_j p_j=\phi_j(0)\,f_{\mathrm{R}}(t)+\sum_{i=1}^{n}\phi_j(x_i)\,f_{\mathrm{d}}(x_i,t)+\sum_{i=1}^{n}\phi_j(x_i)\,f(x_i,t) \tag{32}$$

and the governing equation of the *i*th resonator is given by

$$m_{\mathrm{r}}\ddot{z}_i(t)+f_{\mathrm{d}}(x_i,t)+f(x_i,t)=0 \tag{33}$$

where

$$m_j=\rho A\int_0^L\phi_j^2(x)\mathrm{d}x;\;\; k_j=EI\int_0^L\phi_j^{(4)}(x)\phi_j(x)\mathrm{d}x;\; c_j=2\zeta_j\sqrt{m_j k_j};\; f_{\mathrm{d}}(x_i,t)=2\zeta_{\mathrm{o}}\sqrt{m_{\mathrm{r}}k_{\mathrm{v}}}\left[\dot{z}_i(t)-\sum_{j=1}^{N}\phi_j(x_i)\,\dot{p}_j(t)\right] \tag{34}$$

where ζ_j is the damping ratio of the *j*th beam mode, which is introduced to dampen free vibrations, $f_{\mathrm{d}}(x_i,t)$ is the internal damping force of the *i*th resonator, and ζ_{o} is the damping ratio of the resonator.

The displacements in generalized coordinates and the absolute displacements of all oscillators can be directly obtained by solving simultaneous equations (32) and (33), and then substituting those generalized displacements into Eq. (26) gives the displacement responses of the beam. Note that the number of Galerkin truncation N should be large enough to meet the requirement on computational accuracy.

III. Numerical results

A set of parameters of the HSLDS-LR beam are listed in Table I. The material parameters and a part of geometric parameters of the beam are chosen from Yu et al.[9]. The length of the beam depends on the number of unit cells, namely $L = nl_c$. The stiffness of oblique springs is related to the proportion of residual stiffness η, as determined by Eq. (6), namely k_o=0.5973$(1-\eta)k_v$. The number of unit cells is selected as n=8 here, and the effects of n on band structures and attenuation property will be discussed in the following section. The numerical tests, for analyzing accuracy of the Galerkin method in relation to the number of truncations N, are carried out but are not shown in this paper for brevity, which indicate that N=10 gives results at high computational accuracy, when the number of unit cells is 8 (L=1 m). It also can be attributed to a fact that the 10th natural frequency in such case, i.e. 5484.6 Hz, is much higher than 800 Hz. According to the mechanism of wave attenuation by local resonators, the beginning frequency of the band gap for the LR beam (η=1) are $\omega_{bL}=\sqrt{k_v/m_r}$, and that of the HSLDS-LR beam is expected to be $\omega_{bN}=\sqrt{\eta k_v/m_r}=\sqrt{\eta}\omega_{bL}$, when the resonator undergoes weak oscillations.

TABLE I. Parameters of the HSLDS-LR beam

Parameters	Descriptions	Values
E	Module of elasticity	70 GPa
ρ	Density	2600 kg/m^3
I	Area moment of inertia	5.968×10^{-9} m^4
A	Area	1.602×10^{-4} m^2
l_c	Length of unit cell	0.125 m
m_r	Mass of resonator	0.0437 kg
k_v	Stiffness of vertical spring	1.65×10^5 N/m
l	Length of oblique spring	0.0459 m
$\zeta_j\ (j=1-N)$	Modal damping ratios	0.02
ζ_o	Damping ratio of resonator	0.01
$\mathrm{Ex}(f_R)$	Amplitude Expectation	10 N

It is reminded that the linearized stiffness of the HSLDS resonator, i.e. ηk_v, is used to achieve band structures calculated by Eq. (23). As mentioned previously, there are four solutions of the wave vector q, namely two near-field wave

components dampened within finite distances; and two traveling wave components which pass through the beam when the solutions of q are real, but are dampened when the solutions are imaginary[9]. The band structures are shown in Fig. 3 for different residual stiffness. The solid lines represent the real wave vector q, and the shadow areas denote band gaps (i.e., stop band of flexural wave propagation), in which the wave vector q is imaginary. The beginning and ending frequencies of the band gap versus the proportion of residual stiffness η are depicted in Fig. 4. From Figs. 3 and 4, it can be observed that the band gap is shifted from high frequency range to lower one as η decreases, while the band gap becomes narrow. According to Smith et al.[32], the ending frequency of the band gap can be given by $\omega_{eL}=\omega_r\sqrt{(1+\mu)}$, where $\mu=m_r/\rho Al_c$ is the ratio of the mass of resonator to that of the unit cell of the beam, and $\omega_r=\sqrt{\eta k_v/m_r}$ is the resonant frequency of the HSLDS resonator. Consequently, the band gap becomes narrow as the resonant frequency is changed into low values.

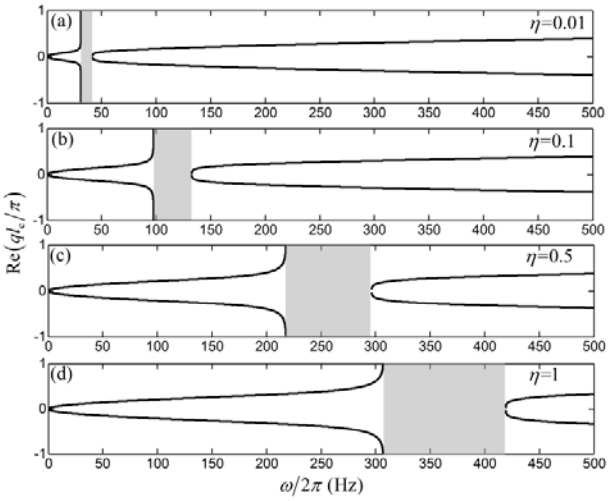

FIG. 3. Band structures calculated by Eq. (23) of the HSLDS-LR beam for different residual stiffness of the HSLDS resonator. (a) η=0.01, (b) η=0.1, (c) η=0.5, (d) η=1. Shadow areas represent band gaps.

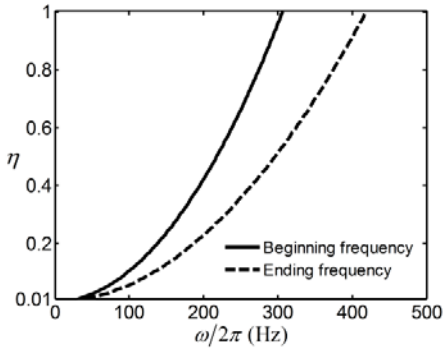

FIG. 4. Beginning frequency (solid line) and ending frequency (dashed line) of the band gap for different residual stiffness of the HSLDS resonator.

Band structures are verified by calculating FRFs, which are obtained by solving simultaneous equations (32) and (33). Note that the original nonlinear stiffness (i.e., Eq. (7)) of the HSLDS resonator is adopted in numerical simulations. Fig. 5 shows FRFs for four cases of residual stiffness, corresponding to the band structures in Fig. 3. One can see excellent agreement between theoretical results and numerical simulations. A contour plot of FRFs versus the proportion of residual stiffness and excitation frequency is depicted in Fig. 6a, where the colored area with values below zero denotes frequency range of the band gap, which is also illustrated as the area surrounded by frequency band-gap edges in Fig. 6b. Comparing this area with that surrounded by the two lines representing the beginning and ending frequencies of the band gap in Fig. 4, one can also observe good agreement. Therefore, the band structures of flexural wave propagation in the HSLDS-LR beam can be effectively predicted by transfer matrix method with the usage of linearized stiffness, as long as the resonator does not undergo large displacements. The effects of excitation amplitudes on band structures will be discussed in the following section.

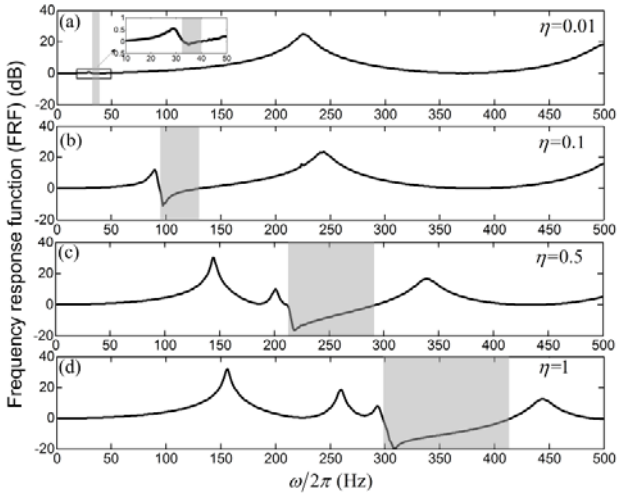

FIG. 5. FRFs of the HSLDS-LR beam calculated by Galerkin method. (a) η=0.01 , (b) η=0.1 , (c) η=0.5 , (d) η=1 . Shadow area denotes the band gap.

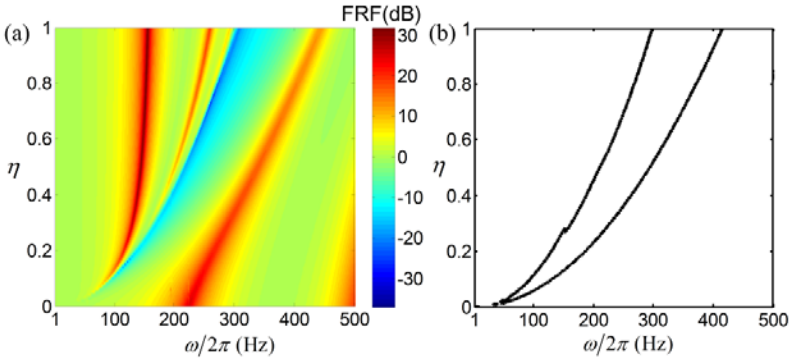

FIG. 6. (a) Contour plot of FRFs (dB) of the HSLDS-LR beam vs the proportion of residual stiffness and excitation frequency; (b) the frequency band-gap edges.

Most importantly, from both the observations of theoretical analysis and numerical simulations, it indicates that adding NS mechanisms to resonators can successfully shift band gaps form high frequency to lower one by a proportion of $\sqrt{\eta}$. As a result, the locations of band gaps can be tuned into desired low frequency ranges by adjusting the stiffness of oblique springs, according to the expression of k_o=0.5973$(1-\eta)k_v$. Indeed, the bandwidth becomes narrow and the attenuation performance deteriorates, as the frequency of the band gap decreases. These issues might be further resolved by using multiple HSLDS resonators with mismatching resonant frequencies or combining with piezoelectric shunts to broaden bandwidth and drop the FRF curves even further.

IV. Further analysis

For a finite-length LR beam, the efficiency of wave attenuation is most likely affected by the number of unit cells[11]. As shown in Fig. 5, the wave attenuation of the HSLDS-LR beam with 8 unit cells degrades as the frequency approaches to the ending frequency of the band gap. Additionally, the stiffness of the HSLDS resonator has a typical feature of nonlinearity, that is, it depends on the magnitude of response, or in other words on the level of excitation. Therefore, to address the above concerns, the effects of the number of unit cells on wave attenuation and what would happen to the band structure under large excitations will be analyzed in this section.

A. Effect of the number of unit cells on wave attenuation

To demonstrate the effects of the number of unit cells on wave attenuation, comparisons of FRFs among n=8, n=16 and n=24 for two cases of residual stiffness, η=0.25 and η=0.75, are shown in Fig. 7. The contour plots of FRFs for different number of unit cells, n=16 and n=24, are depicted in Fig. 8, which presents comprehensive evaluations of FRFs against the residual stiffness and excitation frequency. Note that when the number of unit cells is 24, the length of the beam changes into 3 m, and thus several natural frequencies lower than 800 Hz occur. In order to cover all the natural frequencies lower than 800 Hz, the number of modes N is increased to 15.

It can be seen that more resonant peaks occur as the number of unit cells increases, because more low natural frequencies appear as the length of beam becomes greater. Obviously, in the band gap, the wave attenuation is significantly improved by increasing the number of unit cells. Especially, a sharp drop occurs near the ending frequency of the band gap for large values of η, when n=16 and n=24, as shown in Fig. 7b and Fig. 8. Notice that in Fig. 8 two edges of the band gap region are now in distinct colors, such as dark blue (comparing with Fig. 6), representing better attenuations. Nevertheless, for all values of η, the efficiency of mitigating wave revealed by the FRF is improved notably by the increasing number of

unit cells. Therefore, to filter undesirable vibrations pass through a finite-length beam in practice, a sufficient number of unit cells are needed to achieve a good performance of attenuation.

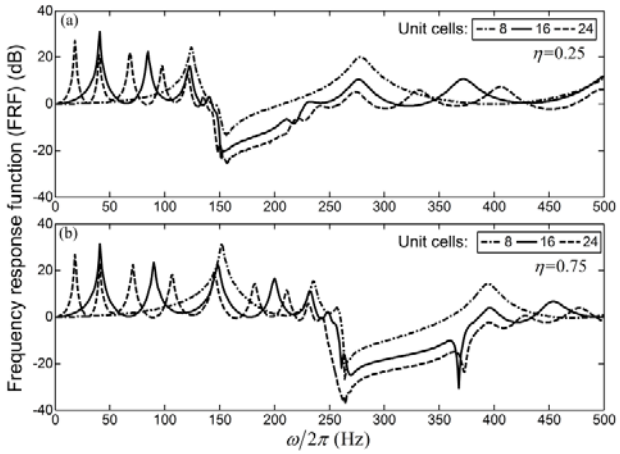

FIG. 7. FRFs of the HSLDS-LR beam with different numbers of unit cells: dash-doted lines, n=8; solid lines, n=16; dashed lines, n=24. (a) η=0.25 , (b) η=0.75 .

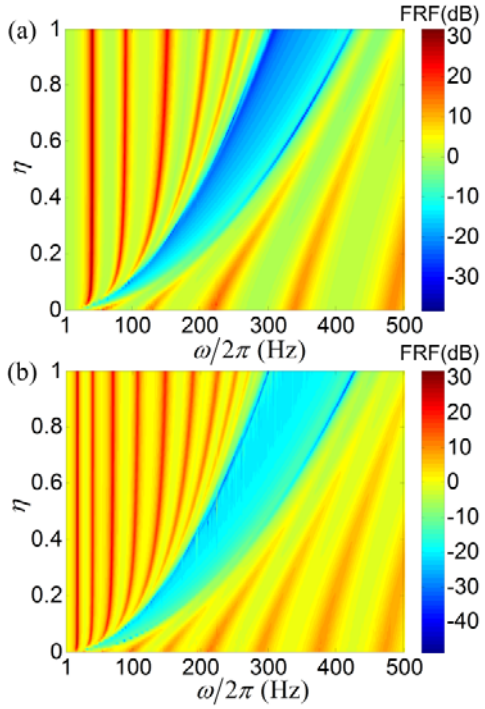

FIG. 8. Contour plots of FRFs (dB) of the HSLDS-LR beam vs the proportion of residual stiffness and excitation frequency for different numbers of unit cells: (a) n=16, (b) n=24.

B. Effect of the excitation amplitude on band structures

As mentioned before, the stiffness of the HSLDS-LR oscillator is nonlinear, and thus it depends on the relative displacement amplitude between the center of the mass and the connecting point on the beam. Under low excitations the relative displacement is small, and the nonlinearity is not notable. However, under large excitations, the nonlinearity cannot be neglected, whose effects on wave attenuation will be analyzed in terms of FRF in the following numerical simulations.

Fig.9 shows contour plots of FRFs excited by the random force for η=0.25 and η=1 . Note that η=1 means no nonlinearity, and it is a case of pure linearity. It can be observed form Fig. 9a that the band gap on the contour plot becomes indistinct as the amplitude expectation of the random force is increased. The reason is that complicated dynamic behavior of a system with strong nonlinearity is readily aroused by the excitation with multiple harmonic components, especially those components with non-commensurate frequencies[33]. Consequently, when the amplitude expectation is relatively large, some harmonic components of the output signal are amplified, but some others are reduced, and even some new components occur. It leads to rapid changes of FRFs with respect to the frequency, and thus the band-gap area becomes indistinct as the random force increases. In contrast, dynamic behavior of a linear system (η=1) cannot be affected by the increasing force, as shown in Fig. 9b, where the band-gap area remains unchanged by the increasing random forces.

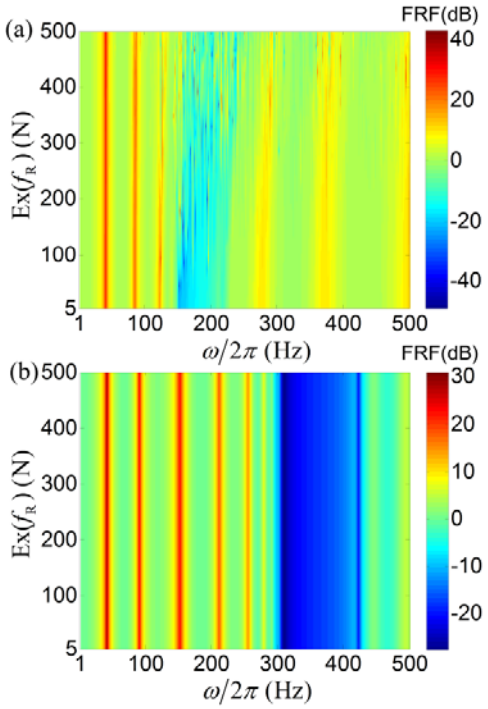

FIG. 9. Contour plots of FRFs (dB) of the HSLDS-LR beam with 16 unit cells vs amplitude expectation and frequency of the random excitation for different proportion of residual stiffness: (a) η=0.25 , (b) η=1 .

Moreover, the dynamic behavior of a strongly nonlinear system under a single-harmonic excitation might be different from those under multi-harmonic excitation. In the case of a single-harmonic excitation $F_0 \cos \omega t$, the FRF is defined by the Root Square Mean (RSM) displacement ratio of the output signal to the input one. Recall that the excitation is acting on the left end of the HSLDS-LR beam, and the time history of displacement of the left end is chosen as the input signal, and that of the right end as the output one. The FRFs for different amplitudes of single-harmonic excitations are shown in Fig. 10, when η=0.25 .

It can be observed that the band gap is shifted to higher frequency by the increasing excitation, which can be attributed to the fact that the stiffness of HSLDS resonator possesses hardening nonlinearity[34], namely its stiffness increases as the displacement is increased. Increase of stiffness implies an alteration of the location of the band gap from low frequency to higher one. Also shown is that the band gap is split into two parts, and the bandwidth with high attenuation (small FRF values) becomes narrow, as shown in Figs. 10c and 10d, which indicates that the efficiency of wave attenuation would get worse under very large excitations.

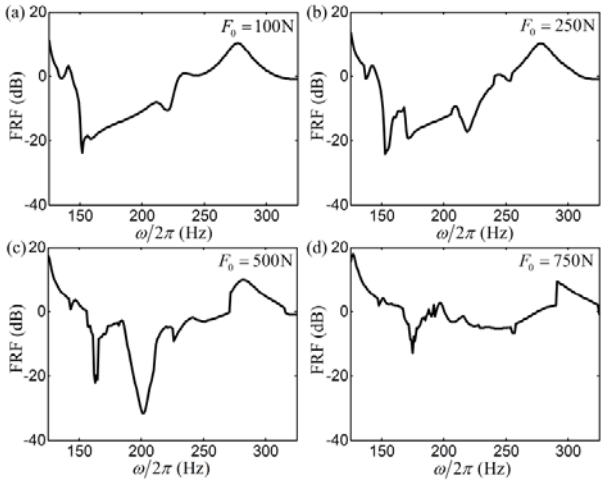

FIG. 10. Effects of excitation amplitude on FRFs of the HSLDS-LR beam with 16 unit cells and η=0.25 . (a) F_0=100N, (b) F_0=250N, (c) F_0=500N, (b) F_0=750N.

It is of interest that the jump phenomenon (Fig. 10d) and chaotic motions (Fig. 11), intrinsic features of nonlinear dynamic systems, are aroused by very large excitations. Fig. 11 depicts time histories of the input and output signals, when $F_0 = 750$N and $\omega = 350\pi$ rad/s , at which a drop of FRF appears (Fig. 10d). Fig. 11b shows a Poincare section of the output signal, from which one can make a judgement that the motion is chaotic, as evidenced by a cloud of points in a Poincare section for a lightly dampened nonlinear system[33]. However, from Fig. 11a, one can still observe a considerable attenuation of wave propagation, even though the responses are chaotic, and the band gap with high efficiency of wave attenuation gets narrow under such large excitations (Fig 10d).

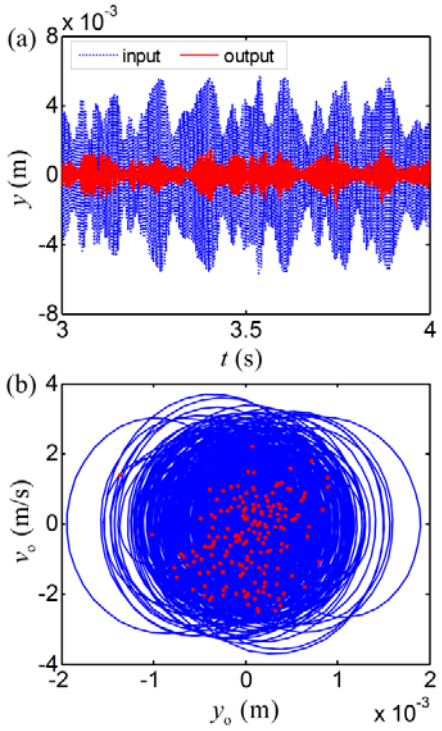

FIG. 11. Response of the HSLDS-LR beam with 16 unit cells when F_0=750N and ω=350π rad/s . (a) Time histories of input signal (dotted line) and output signal (solid line), (b) Poincare section of the output signal.

V. CONCLUSION

In this paper, a new local resonator with high-static-low-dynamic stiffness (HSLDS) is proposed to shift the band gap of flexural wave in beams into lower frequency range by adding negative-stiffness (NS) mechanisms. The band structures of flexural wave propagation in a HSLDS-LR beam with infinite length are obtained by using the transfer matrix method, when the linearized stiffness is used in the case of small-amplitude oscillations, which are verified by numerical simulations of a HSLDS-LR beam with finite length under free-free boundary condition. The effects of the number of unit cells on wave attenuation, and the impacts of the excitation amplitude on band structures are discussed. Several conclusions can be drawn as follows.

The stiffness of the HSLDS resonator can be reduced effectively by connecting in parallel two oblique springs that provide negative stiffness, which implies that the resonant frequency of the resonator can be decreased substantially, and thus the band gap can be shifted into lower frequency range. It is of interest to stress that the band gap can be assigned to a desired location by tuning only the stiffness of oblique springs. The efficiency of wave attenuation is improved notably by the increasing number of unit cells for HSLDS-LR beams with finite length. Therefore, a sufficient number of unit cells are needed to achieve a good performance of filtering undesirable flexural waves. Moreover, the band gap is shifted to a higher

frequency by the increasing excitation. Especially, under large excitations, the band gap becomes narrow, and the efficiency of wave attenuation gets worse, due to complicated dynamic behaviors induced by the nonlinearity of the HSLDS resonator.

ACKNOWLEDGMENTS

This research work was supported by National Natural Science Foundation of China (11572116), Natural Science Foundation of Hunan Province (2016JJ3036), and Fundamental Research Funds for the Central Universities. This work is carried out during the first author's visit to the University of Liverpool.

REFERENCES

1. L. Brillouin, *Wave Propagation in Periodic Structures: Electric Filters and Crystal Lattices*. (Dover Publications, Inc., New York, 1946).
2. M. M. Sigalas and E. N. Economou, Journal of Sound and Vibration **158** (2), 377-382 (1992).
3. M. S. Kushwaha, P. Halevi, L. Dobrzynski and B. Djafari-Rouhani, Physical Review Letters **71** (13), 2022-2025 (1993).
4. D. M. Mead, Journal of Sound and Vibration **190** (3), 495-524 (1996).
5. Z. Liu, X. Zhang, Y. Mao, Y. Y. Zhu, Z. Yang, C. T. Chan and P. Sheng, Science **289** (5485), 1734-1736 (2000).
6. S. Mohammadi, A. A. Eftekhar, W. D. Hunt and A. Adibi, Applied Physics Letters **94** (5), 051906 (2009).
7. M. I. Hussein, M. J. Leamy and M. Ruzzene, Applied Mechanics Reviews **66** (4), 040802-040802 (2014).
8. P. A. Deymier, *Acoustic Metamaterials and Phononic Crystals*. (Springer, Heidelberg, 2013).
9. D. Yu, Y. Liu, G. Wang, H. Zhao and J. Qiu, Journal of Applied Physics **100** (12), 124901 (2006).
10. D. Yu, Y. Liu, H. Zhao, G. Wang and J. Qiu, Physical Review B **73** (6), 064301 (2006).
11. Y. Liu, D. Yu, L. Li, H. Zhao, J. Wen and X. Wen, Physics Letters A **362** (5–6), 344-347 (2007).
12. Y. Xiao, J. Wen, D. Yu and X. Wen, Journal of Sound and Vibration **332** (4), 867-893 (2013).
13. J. S. Chen, B. Sharma and C. T. Sun, Composite Structures **93** (8), 2120-2125 (2011).
14. Y. Xiao, J. Wen and X. Wen, Physics Letters A **376** (16), 1384-1390 (2012).
15. R. Zhu, X. N. Liu, G. K. Hu, C. T. Sun and G. L. Huang, Journal of Sound and Vibration **333** (10), 2759-2773 (2014).
16. M. Badreddine Assouar and M. Oudich, Applied Physics Letters **100** (12), 123506 (2012).
17. Y. Xiao, J. Wen, G. Wang and X. Wen, Journal of Vibration and Acoustics **135** (4), 041006-041006 (2013).
18. M. Y. Wang, Y. T. Choy, C. W. Wan and A. S. Zhao, Journal of Vibration and Acoustics **137** (6), 064504-064504 (2015).
19. X. Wang and M. Y. Wang, Meccanica **51** (1), 171-178 (2016).
20. P. F. Pai, H. Peng and S. Jiang, International Journal of Mechanical Sciences **79**, 195-205 (2014).
21. T. Wang, M.-P. Sheng and Q.-H. Qin, Physics Letters A **380** (4), 525-529 (2016).
22. F. Casadei, M. Ruzzene, L. Dozio and K. A. Cunefare, Smart Materials and Structures **19** (1), 015002 (2010).
23. A. Spadoni, M. Ruzzene and K. A. Cunefare, Journal of Intelligent Material Systems and Structures (2009).
24. O. Mourad, L. Yong, M. A. Badreddine and H. Zhilin, New Journal of Physics **12** (8), 083049 (2010).

25. M. Oudich, M. Senesi, M. B. Assouar, M. Ruzenne, J.-H. Sun, B. Vincent, Z. Hou and T.-T. Wu, Physical Review B **84** (16), 165136 (2011).
26. M. Nouh, O. Aldraihem and A. Baz, Journal of Vibration and Acoustics **136** (6), 061012-061012 (2014).
27. O. R. Bilal and M. I. Hussein, Applied Physics Letters **103** (11), 111901 (2013).
28. M. Badreddine Assouar, J.-H. Sun, F.-S. Lin and J.-C. Hsu, Ultrasonics **54** (8), 2159-2164 (2014).
29. Q. Cao, M. Wiercigroch, Pavlovskaia, E. E, C. Grebogi, T. Thompson and J. Michael, Physical Review E **74** (4), 046218 (2006).
30. A. Carrella, M. J. Brennan and T. P. Waters, Journal of Sound and Vibration **301** (3-5), 678-689 (2007).
31. S. S. Rao, *Mechanical Vbrations, Fourth Edition* . (Prentice Hall, 2003).
32. T. L. Smith, K. Rao and I. Dyer, Noise Control Engineering Journal **26**, 56-60 (1986).
33. F. C. Moon, *Chaotic Vibrations: An Introduction for Applied Scientists and Engineers*. (John Wiley & Sons, New York, 1987).
34. A. H. Nayfeh and D. T. Mook, *Nonlinear Oscillations*. (John Wiley & Sons, Inc., New York, 1995).